Chapter

Plasma Diagnostic Methods: Test Charge Response in Lorentzian Dusty Plasmas

Shahid Ali and Yas Al-Hadeethi

Abstract

Different plasma diagnostic methods are briefly discussed, and the framework of a test charge technique is effectively used as diagnostic tool for investigating interaction potentials in Lorentzian plasma, whose constituents are the superthermal electrons and ions with negatively charged dust grains. Applying the space-time Fourier transformations to the linearized coupled Vlasov-Poisson equations, a test charge potential is derived with a modified response function due to energetic ions and electrons. For a test charge moving much slower than the dust-thermal speed, there appears a short-range Debye-Hückel (DH) potential decaying exponentially with distance and a long-range far-field (FF) potential as the inverse cube of the distance from test charge. The FF potentials exhibit more localized shielding curves for low-Kappas, and smaller effective shielding length is observed in dusty plasma compared to electron-ion plasma. However, a wakefield (WF) potential is formed behind the test charge when it resonates with dust-acoustic oscillations, whereas a fast moving test charge leads to the Coulomb potential having no shielding around. It is revealed that superthermality and plasma parameters significantly alter the DH, FF, and WF potentials in space plasmas of Saturn's E-ring, where power-law distributions can be used for energetic electrons and ions in contrast to Maxwellian dust grains.

Keywords: kinetic model, test charge technique, DA waves, superthermal tails, dynamical shielding

1. Plasma diagnostic methods

To understand a plasma state and its characteristics, numerous experimental techniques, mechanisms, devices, theoretical models, and computational packages have been developed as diagnostic tools for measuring the plasma parameters such as the plasma electron density and temperature [1, 2] as well as their spatial profiles and dynamics. These diagnostic techniques are used to adequately describe both low-temperature and high energy density plasmas. In some situations, the measurements by these techniques cause perturbations in plasmas and are termed as active diagnostic techniques, while passive ones do not perturb plasmas. Based on the degree of ionization, the plasmas can broadly be classified into cold and hot plasma states, which accordingly demand for various types of diagnostics to

precisely estimate the plasma parameters for optimal understanding of the physics of plasmas. This includes both theoretical and experimental findings. The most common techniques for cold and hot plasmas ($T_e \geq$ few keV) are the Langmuir probes in the form of planar, cylindrical, or spherical electrodes in plasmas with a goal to monitor the plasma parameters. The probes can be of several types, namely, single and/or double probes, which are used for density, temperature, and floating potential measurements. Emissive and magnetic probes work more efficiently for plasma potential measurement and wave field amplitude and phase diagnostics, respectively, while the Rogowski for antenna current measurements. There are many complications, for example, the plasma potential and density can fluctuate or drift during the time of probe measurements. In some complications, since the probe draws a large amount of currents from a plasma and perturbs the initial state of the plasma, it may lead to the erroneous measurements; even then, the Langmuir probe diagnostics are widely used and this is because of the fact that they are relatively simple to use, cheap, and give reliable values of important plasma parameters.

On the other hand, in certain plasma sources like tokamak plasmas, strong currents are generated, which give rise to various kinds of magnetohydrodynamic (MHD) instabilities. For this, a magnetic probe is used, which is beneficial especially for measuring either local magnetic fields or its fluctuations not only in tokamaks but also in laser-produced plasmas (LPP). Furthermore, the amplitude of current flowing into the plasma can be estimated by integrating the induced magnetic field around the plasma column by utilizing the so-called Rogowski coil. However, in some plasmas (especially high temperature), it is not feasible to utilize material probes for determining the plasma parameter like plasma electron density. Therefore, a nonperturbing approach is needed to diagnose the plasma. In such a scenario, the electromagnetic spectrum is utilized. But the electromagnetic wave intensity must be low enough to the level that it will not result in plasma perturbation. For probing the high-density plasmas, a lower wavelength is required as a probe. This justifies the utilization of infrared radiation in tokamak and ultraviolet radiation for measuring the plasma electron density in LPP. The variation of the polarizing angle involving the beam probe in the presence of magnetic field can also be used for diagnostics of tokamak plasmas.

Interestingly, the evaluation of appropriate plasma parameters may be carried out by spectroscopy of emitted radiations as used generally from the beginning of plasma physics. This technique for emission measurements has been particularly making significant contributions over the past five decades for the fact that plasmas produced for nuclear fusion research exhibit intense emission in the X-ray region. Astrophysical applications further justify the wide interest in X-ray emission from plasmas. The phase soft X-ray (so defined due to their low penetrating power) indicates electromagnetic radiations with a wavelength in range $1\text{Å} \leq \lambda \leq 300\text{Å}$ (or, in terms of photon energy $h\nu$, 300 eV $\leq h\nu \leq$ 10 keV). Hard X-rays below 1 Å are occasionally produced in plasmas for highly accelerated electrons, like runaway electrons in tokamak plasmas and suprathermal electrons in LPP [3]. The characteristics of soft X-ray spectra like line intensities, line profiles, and continuum intensities can be investigated to determine the electron densities by Stark broadening, while the ion densities from the absolute radiation intensities and ion temperatures using the Doppler broadening of spectral lines [2].

The particle measurement method is another scheme for investigating the characteristics of plasmas by using the beam of fast particles. It has received much attention in the studies of inertial confinement fusion and energy deposition in a medium driven by cluster-ion and fast heavy-ion beams, as well as in plasma accelerators and low-temperature laboratory plasmas.

2. Dusty plasma and test charge technique

The most common ingredient of astrospace plasmas is the dust component in addition to electrons and ions, found everywhere in earth atmospheres, in comets, in planetary rings, in interstellar clouds, in interplanetary space, in interstellar medium, etc. Dust grains may exist in the form of ice particles, metallic and dielectric materials, and are highly charged species due to different charging processes. For instance, the absorption of ambient electrons and ions on dust grain surface may lead to the negatively charged dust grains, while thermionic and secondary electron emissions as well as ultraviolet photoionization give rise to positively charged dust grains. Thus, a multispecies dusty plasma can be assumed as more complex plasma than conventional electron-ion plasma, for dust size, mass, and charge variations. Being an abundant component of the space and industrial plasmas [4, 5], dusty plasma has always attracted lots of interests for studying new distinct features of plasma modes [6, 7] with a static and dynamic background of dust grains both analytically and experimentally [8–10]. Numerous linear and nonlinear [viz., solitons, shocks, vortices, etc.] dusty modes and associated instabilities are investigated using the frameworks of perturbative and nonperturbative schemes.

The behavior of charged particles in plasmas can be described by the well-known fluid and kinetic theories [4, 11], essentially helpful for studying the basic properties of plasma waves and instabilities, depending strongly on the observed phenomena. Laboratory plasmas have effectively been modeled by fluid description, where charged fluids of plasma species are assumed in temporal and spatial configurations. But, it has been observed that fluid theory does not account for velocity space coordinate and is insufficient to study the wave phenomena in non-equilibrium plasmas, where particle distributions show significant deviations from the equilibrium states. Hence, fluid theory is unable to explain the wave-particle interactions that could lead to collisionless Landau damping phenomenon and many other interesting features of collective modes and instabilities. Conversely, kinetic theory adequately describes the physical phenomena in real time and phase space configurations, providing all information about plasma waves, instabilities, plasma equilibrium, Landau damping rate, etc.

Test charge techniques [12, 13] can be utilized to study the shielding of test charges in collisional [14] and turbulent [15] plasmas, the electric field [16], and far-field potential of a test charge in a nonuniform magnetoplasma [17], the wake-field excitations in charge fluctuating dusty plasmas [18], the two-body correlations [19], the energy loss of test charges [20], etc. If a test particle is projected into the plasma with a constant speed, its charge density is coupled with the plasma charge density by the space charge effects. Consequently, the test charge is screened by a cloud of opposite sign charges leading to the short-range Debye-Hückel (DH) potential. Of course, the speed of test charge significantly matters in plasmas when it is considered with respect to thermal speeds of plasma species. The interaction potentials and energy loss of charged particles have been recognized in many research areas, for example, in ion-cluster interaction with condensed matter [21, 22], in inertial confinement fusion [23–25], in particle acceleration [26], in low-temperature laboratory plasmas [27, 28], and in dense plasmas for heavy-ion energy deposition [29].

Montgomery et al. [13] employed the test charge technique to obtain far-field potential distribution around a test charge, which decays as the inverse cube of the distance from test charge in electron-ion Maxwellian plasmas. Subsequent investigations of shielded potentials have been phenomenally influenced by the ionic motion [30], electron-electron collisions [14, 31], and plasma turbulence [15]. The electrostatic potential [32] due to small and large test charge velocities has been

investigated to display the excitation of long-range wakefields in Maxwellian plasmas. Shivamoggi and Mulser [33] examined the effects of magnetic field, collisions, and plasma inhomogeneity on the potential due to slowly and rapidly moving test charges [17, 34], and Lakshmi et al. [35] discussed the Debye shielding phenomenon in a dusty plasma by considering the Boltzmannian electrons and ions with cold negative dust grains. It was revealed that plasma parameters significantly alter the characteristics of small and large amplitude potentials. Later, Shukla [36] reported the FF potential for a slowly moving test charge in a Maxwellian dusty plasma and showed the impact of dust-charge variation on the dipole-like FF potential. Moreover, oscillatory wake-field can be excited behind the test charge [37] in a collisionless unmagnetized plasma with Maxwellian electrons and ions. Nambu et al. [38] extended this work to dusty plasmas and explained the resonant phenomenon of DA waves with a test charge, resulting in the long-range WF potential. Later, Shukla and Rao [39] analyzed the WF, DH, and FF potentials of test charge in a colloidal Maxwellian plasma accounting for the streaming ions and dust grains. It was found that external magnetic field and ion-streaming effects [40, 41] strongly affect the positive/negative potential regions in plasmas. To explore the effects of two-body correlations, dust-charge perturbations and dust-neutral collisions, various geometries have been designed for propagating test charges [18–20] in an unmagnetized Maxwellian dusty plasma. In all above investigations, the plasma particles are described by the Maxwellian distribution function.

The shielding phenomenon is one of the main objectives of this chapter to unfold many intrinsic properties of the Lorentzian space dusty plasma, which discerns it from the standard Maxwellian plasmas. It plays a key role in setting up the basic criteria for Lorentzian dusty plasmas. Any plasma medium can physically be polarized by the test charge to give rise to perfect screening if thermal agitations are absent in the plasma system. Conversely, an imperfect shielding occurs if the plasma particles get enough thermal energy to escape from the edge of screening cloud. The interaction potentials caused by the test charge are not only strongly influenced by different test charge speeds in comparison with the thermal speeds but also lead to the possibility of dust crystallization and dust coagulation in space Lorentzian dusty plasmas.

3. Power-law Lorentzian distribution function (df)

In some circumstances, the behavior of plasma particles cannot be described by the usual Maxwellian distribution function (df) but often modeled by the power-law df. When all or some of the plasma particles move faster than their thermal speeds, the plasma particles are known as superthermal/suprathermal species, showing high energy and velocity tails in the distribution. They are mostly accelerated by wave-particle interactions, modulational instabilities and Langmuir turbulence [42], beam-plasma interactions [43], solar wind where type III solar radio emissions occurs [44], intense microwave-plasma interactions [45], ionospheric heating experiments [46], etc. Recognizing the role of superthermal energetic particles in plasmas, the wave dynamics and instabilities need to be re-investigated with a power-law df that gives a better fit to empirical data from space plasmas. A 3D isotropic Kappa-df [47] for superthermal particles can be expressed as

$$f_{s0}^{K}(\mathbf{v}_s) = A_{\kappa_s}\left(1+\frac{v_s^2}{\kappa_s\theta_{Ts}^2}\right)^{-\kappa_s-1}. \tag{1}$$

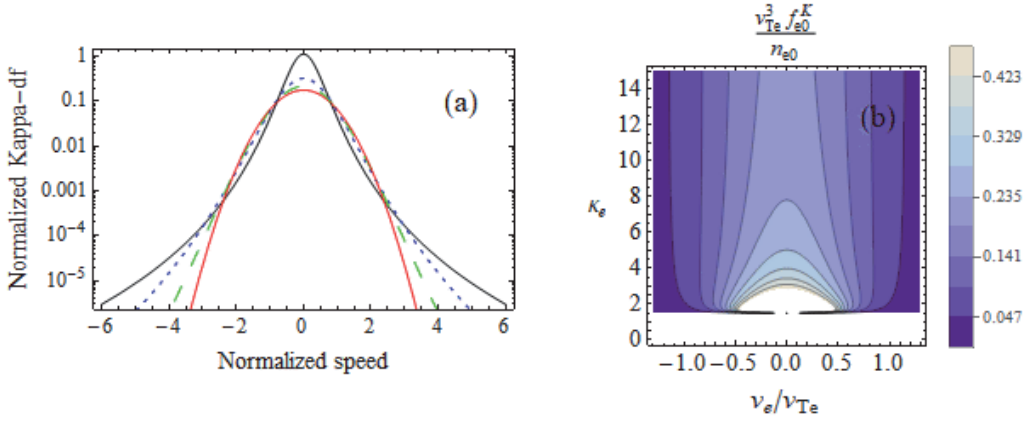

Figure 1.
Kappa-df against the electron speed for different values of kappa index both in 2D and in contour plots. In (a), the solid-black, dotted-blue, dashed-green, and solid-red curves correspond to $\kappa_e = 2$, 4, 10, and $\kappa_e \to \infty$, respectively. However, in (b), the light colors indicate more number of electrons and vice versa for dense colors.

The normalization constant and effective thermal speed are denoted by $A_{\kappa_s} = n_{s0}\pi^{-3/2}\kappa_s^{-3/2}\theta_{Ts}^{-3}\,\Gamma(\kappa_s+1)/\Gamma(\kappa_s-1/2)$ and $\theta_{Ts} = \{2(\kappa_s-3/2)/\kappa_s\}^{1/2}(T_s/m_s)^{1/2}$, respectively. The symbol Γ indicates the Gamma function, and $\mathbf{v}_s$ and n_{s0} are the velocity and equilibrium number density, whereas T_s (m_s) stands for the temperature (mass) of the *sth* species ($s = e$ for electrons and i for positive ions). The effective thermal speed θ_{Ts} is always realistic in the limit $\kappa_s > 3/2$, where κ_s is the spectral index showing the deviation from the Maxwellian df. **Figure 1** displays the normalized Kappa-df [as given by Eq. (1)] for the electrons as function of normalized electron speed with varying κ_e-index both in 2D and contour plots. See that superthermal electrons exhibit high energy tails at $\kappa_e = 2$, 4, and 10 in distribution curves, which tend to the Maxwell-Boltzmann distribution curve for $\kappa_e \to \infty$. Therefore superthermality effects are only significant for low values of Kappa, and for its infinite values, the Kappa-df exactly converges to the Maxwell-df $\left[viz., f_{s0}^K(\mathbf{v}_s) \to f_{s0}^M(\mathbf{v}_s)\right]$. It may be noted from contours (see **Figure 1(b)**) that light-colored regions correspond to more electrons at low speeds, and while moving toward the dense-colored regions, the number of electrons decreases but comparatively has high speeds. In 1968, for the first time, Vasyliunas [47] pointed out the implications of Kappa-df by fitting empirical data from solar wind and showed the significance of low values of electron spectral index, that is, $\kappa_{s=e} \sim 2-4$. The effects of high energy tails have significantly modified the dispersive properties of waves and instabilities [48, 49] in Lorentzian plasmas. Recently, Ali and Eliasson [50] investigated the impact of suprathermal hot electrons on the electrostatic potential of slowly moving test charge in a two-temperature electron plasma and extended the model for Lorentzian dusty plasmas [51].

4. Kinetic model for Lorentzian dusty plasmas

To compute the potential distributions around a test charge, we consider a collisionless Lorentzian dusty plasma, containing the suprathermal electrons and ions with negatively charged dust grains following the Maxwell-df. The plasma is also assumed to be field-free in the sense that there is no external electric or magnetic field (viz., $E_0 = 0 = B_0$), so that the equilibrium electrostatic potential $\phi_0 = 0$. The quasi-neutrality condition at equilibrium demands $n_{e0} = n_{i0} - Z_{d0}n_{d0}$, where Z_{d0}

being the equilibrium dust-charge state and n_{j0} denote the particle number densities of the jth species [j equals $s(=e,i)$ for Kappa-distributed electrons and ions while $j=d$ for negatively charged dust grains]. In this model, all the dust grains are assumed to be spherical in shape with constant size of radius r_d and mass m_d.

The Lorentzian dusty plasma in the presence of a test charge can be described by the following linearized coupled set of Vlasov-Poisson equations:

$$(\partial_t + \mathbf{v}_d \cdot \nabla) f_{d1} + \frac{q_{d0}}{m_d} \mathbf{E}_1 \cdot \nabla_{\mathbf{v}_d} f_{d0}^M = 0, \tag{2}$$

$$(\partial_t + \mathbf{v}_s \cdot \nabla) f_{s1} + \frac{q_s}{m_s} \mathbf{E}_1 \cdot \nabla_{\mathbf{v}_s} f_{s0}^K = 0, \tag{3}$$

and

$$\nabla^2 \phi_1 + 4\pi \left(\sum_{s=e,i} \rho_s + \rho_d + \rho_T \right) = 0, \tag{4}$$

where $\mathbf{E}_1(=-\nabla\phi_1)$ is the induced electric field with perturbed potential ϕ_1, $q_{d0}(=-Z_{d0}e)$ is the charge of the negative dust grains, and $q_s(=-e,e)$ being the charge of electrons and positive ions. $\rho_d = q_{d0}\int f_{d1} d\mathbf{v}_d$, $\rho_s = q_s \int f_{s1} d\mathbf{v}_s$, and $\rho_T = q_T \delta(\mathbf{r} - \mathbf{v}_T t)$ identify the dust-charge density, electron-ion charge densities, and test charge density, respectively. The symbol δ stands for a 3D Dirac's delta function, and $f_{d0}^M(\mathbf{v}_d)$ and $f_{s0}^K(\mathbf{v}_s)$ are the Maxwell-df and Kappa-df with their perturbed parts $f_{d1}(\mathbf{r},\mathbf{v}_d,t)$ and $f_{s1}(\mathbf{r},\mathbf{v}_s,t)$, such that $|f_{d1}| \ll f_{d0}^M$ and $|f_{s1}| \ll f_{s0}^K$. Also note that test particle has a charge q_T which moves with a constant velocity $\mathbf{v}_T$ along the z-axis in a Lorentzian dusty plasma.

Taking space–time Fourier analysis of Eqs. (2), (3), and (4), we obtain the Fourier transformed potential in this form

$$k^2 D(\mathbf{k},\omega)\phi_1(\mathbf{k},\omega) = 8\pi^2 q_T \delta(\omega - \mathbf{k}\cdot\mathbf{v}_T). \tag{5}$$

The modified longitudinal dielectric constant can be defined by

$$D(\mathbf{k},\omega) = 1 + \sum_s \frac{\omega_{ps}^2}{k^2} \int \frac{\mathbf{k}\cdot\nabla_{\mathbf{v}_s} f_{s0}^K(\mathbf{v}_s)}{(\omega - \mathbf{k}\cdot\mathbf{v}_s)} d\mathbf{v}_s + \frac{\omega_{pd}^2}{k^2} \int \frac{\mathbf{k}\cdot\nabla_{\mathbf{v}_d} f_{d0}^M(\mathbf{v}_d)}{(\omega - \mathbf{k}\cdot\mathbf{v}_d)} d\mathbf{v}_d, \tag{6}$$

where $\omega(k)$ being the angular frequency (wave number) and $\omega_{pj} = \left(4\pi q_j^2 n_{j0}/m_j\right)^{1/2}$ is the plasma oscillation frequency. It is important to mention that if Lorentzian dusty plasma does not contain any test charge, viz., $q_T = 0$, then Eq. (5) simply implies that $D(\mathbf{k},\omega) = 0$, showing a modified linear dispersion relation of electrostatic waves to account for superthermal electrons and ions. However, the inverse Fourier analysis of Eq. (5) leads to the standard form of electrostatic potential due to a test charge in a dusty plasma [11, 32].

$$\phi_1(\mathbf{r},t) = \frac{q_T}{2\pi^2} \int \frac{d\mathbf{k}}{k^2} \frac{\exp\left[i\mathbf{k}\cdot(\mathbf{r} - \mathbf{v}_T t)\right]}{D(k,\mathbf{k}\cdot\mathbf{v}_T)}. \tag{7}$$

The dielectric constant in terms of dielectric susceptibilities $\left(\text{viz., } D = 1 + \sum_{s=e,i} \chi_s + \chi_d\right)$ can be expressed as

$$D(k,\mathbf{k}\cdot\mathbf{v}_T)=1+\sum_{s=e,i}\frac{1}{k^2\lambda_{Ds}^2}\left\{1-\frac{1}{2\kappa_s}+C_sZ_{\kappa_s}(C_s)\right\}+\frac{1}{k^2\lambda_{Dd}^2}\{1+C_dZ_M(C_d)\},\quad(8)$$

where $\lambda_{Ds}\left(=\theta_{Ts}/\sqrt{2}\omega_{ps}\right)$ and $\lambda_{Dd}\left(=v_{Td}/\omega_{pd}\right)$ are the Debye shielding lengths associated with the electron-ion effective speed θ_{Ts} and dust thermal speed $v_{Td}=(T_d/m_d)^{1/2}$. The standard plasma dispersion functions for Kappa-distributed electrons and ions [48] and for Maxwellian dust grains [52], respectively, can be given by

$$Z_{\kappa_s}(C_s)=\frac{1}{\sqrt{\pi}}\frac{\Gamma(\kappa_s+1)}{\kappa_s^{3/2}\Gamma(\kappa_s-1/2)}\int_{-\infty}^{\infty}d\beta_s\frac{\left(1+\beta_s^2/\kappa_s\right)^{-\kappa_s-1}}{(\beta_s-C_s)},\quad \mathrm{Im}(C_s)>0,$$

and

$$Z_M(C_d)=\frac{1}{\sqrt{\pi}}\int_{-\infty}^{\infty}d\beta\frac{\exp\left(-\beta^2\right)}{(\beta-C_d)},\quad \mathrm{Im}(C_d)>0,$$

with their corresponding arguments $C_s=\mathbf{k}\cdot\mathbf{v}_T/\sqrt{2}|k|\theta_{Ts}$ and $C_d=\mathbf{k}\cdot\mathbf{v}_T/\sqrt{2}|k|v_{Td}$.

To proceed further, we shall consider two limiting cases of Eq. (8) by imposing certain limitations on the test charge speed in comparison with the thermal and acoustic speeds and simplify the interaction potentials [as given by Eq. (7)] in Lorentzian dusty plasmas.

4.1 Slow moving test charge response

For a slow test charge propagation in a Lorentzian dusty plasma, we assume that test charge speed (v_T) is much slower than the dust thermal speed (v_{Td}). As a result, the test charge is shielded by all the plasma species, for example, electrons, ions, and dust grains. Since mass of the dust grains is larger than the mass of electrons and ions, therefore the dust thermal speed is much smaller than the electron and ion thermal speeds. Thus, imposing the inequalities $v_T\ll v_{Td}\lll\theta_{Ts}$, we consider only small argument expansions, that is, $|C_s|\ll 1$ and $|C_d|\ll 1$, in the plasma dispersion functions to obtain a simplified expression for dielectric constant. The inverse of the latter eventually yields the following result

$$D^{-1}\simeq\frac{k^2\lambda_{D\kappa}^2}{k^2\lambda_{D\kappa}^2+1}-i\frac{\mu v_T}{v_{Td}}\left(\frac{\pi}{2}\right)^{1/2}\frac{k^2\lambda_{D\kappa}^4}{\lambda_{Dd}^2\left(k^2\lambda_{D\kappa}^2+1\right)^2}.\quad(9)$$

The modified effective Debye length $\lambda_{D\kappa}$ can be simplified in this form

$$\lambda_{D\kappa}=\lambda_0\left(c_{\kappa e}\frac{n_{e0}}{n_0}+c_{\kappa i}\frac{T_e}{T_i}+Z_{d0}^2\frac{n_{d0}}{n_0}\frac{T_e}{T_d}\right)^{-1/2},\quad(10)$$

with superthermality parameters attributed to electrons and ions as

$$c_{\kappa e}=\frac{2\kappa_e-1}{2\kappa_e-3}\quad\text{and}\quad c_{\kappa i}=\frac{2\kappa_i-1}{2\kappa_i-3}.$$

The usual Debye length in electron-ion plasma is denoted by $\lambda_0=(T_e/4\pi n_0e^2)^{1/2}$ with $n_0=n_{i0}\equiv n_{e0}+Z_{d0}n_{d0}$ and $\mu(=\cos\theta_k)$ representing the angle between the

vectors $\mathbf{k}$ and $\mathbf{v}_T$. For Maxwellian plasmas, the superthermality parameters $c_{\kappa e,i} \to 1$ as long as $\kappa_{e,i} \to \infty$, implying that the effective shielding length exactly coincides with the earlier result [35] for static cold dust grains. It may be noticed from Eq. (9) that the inverse of dielectric constant is significantly influenced by the dust Landau damping rate [13]. The importance of the latter was first pointed out [13] in 1968, and it was suggested that if a test charge moves slowly in comparison to the dust thermal speed, the dust Landau damping term appearing in Eq. (9) cannot be ignored. For a static test charge, we set $v_T = 0$ and insert Eq. (9) into Eq. (7) to derive the short-range DH potential [53, 54] in the form $\phi_{DH} = \left(q_T/|r|\right) \exp\left(-|r|/\lambda_{D\kappa}\right)$, where $|r| = \left(\rho^2 + \xi^2\right)^{1/2}$ is the distance from the test charge to an observer in terms of radial and axial distances ρ and $(\xi = z)$, respectively.

For numerical analyses, we can choose the data from the dusty plasma near Saturn's E ring, cited in Refs. [55–58] and many references therein. The data essentially corresponds to the Radio and Plasma Wave Science (RPWS) instruments onboard the Cassini spacecraft, containing the plasma parameters, such as $n_{d0} = 0.1\text{cm}^{-3}$, $n_{e0} = 70\text{cm}^{-3}$, $Z_{d0} = 300$, $T_d = T_e/10$, $T_i = T_e/2$, and $T_e = 4.642 \times 10^5\text{K}$. The computation further helps us in finding the magnitude of the effective shielding length $\lambda_{D\kappa}(= 15.649\text{cm})$ at the near-Maxwellian electrons and ions with $\kappa_{i,e} = 100$. The impact of superthermal tails in the electron and ion distributions only appear at lower values of the Kappa that may result into the reduction of the shielding length $\lambda_{D\kappa} \approx 15.4787\text{cm}$ for fixed $\kappa_i = 1.6$ and $\kappa_e = 100$, as well as $\lambda_{D\kappa} \approx 15.5888\text{cm}$ with $\kappa_e = 1.6$ and $\kappa_i = 100$. Thus, we notice from **Table 1** that for infinite values of the spectral indices, that is, $\kappa_{e,i} \to \infty$, the superthermality parameters $(c_{\kappa e,i})$ tend to unity, implying that the effective shielding length exactly coincides with the previous results [35] for static cold dust grains. However, the variation due to superthermal electrons and ions is shown in three different combinations (see **Table 1**) to affect the normalized values of the effective Debye length and DH potential almost 4 digits beyond the decimal point. At lower Kappa-values, the impact is relatively enhanced and in turn, suprathermal ions more efficiently modify the effective shielding length and DH potential as compared to suprathermal electrons because the ions may take

S #	Spectral-index for electrons κ_e	Spectral-index for ions κ_i	Electron-superthermality parameter c_{κ_e}	Ion-superthermality parameter c_{κ_i}	Effective Debye length $\frac{\lambda_{D\kappa}}{\lambda_0}$	DH Potential $\frac{\Phi_{DH}}{(q_T/\lambda_0)}$
1	100	100	1.01015	1.01015	0.0332829	0.0122817
2	6	100	1.22222	1.01015	0.0332802	0.0122756
3	4	100	1.4	1.01015	0.0332779	0.0122705
4	3	100	1.66667	1.01015	0.0332745	0.0122629
5	2	100	3	1.01015	0.0332573	0.0122249
6	1.6	100	11	1.01015	0.0331548	0.0119997
7	100	100	1.01015	1.01015	0.0332829	0.0122817
8	100	6	1.01015	1.22222	0.03322751	0.0122644
9	100	4	1.01015	1.4	0.0332686	0.0122499
10	100	3	1.01015	1.66667	0.0332588	0.0122281
11	100	2	1.01015	3	0.0332098	0.0121203
12	100	1.6	1.01015	11	0.0329206	0.0114957
13	100	100	1.01015	1.01015	0.0332829	0.0122817
14	6	6	1.22222	1.22222	0.0332724	0.0122583
15	4	4	1.4	1.4	0.0332636	0.0122387
16	3	3	1.66667	1.66667	0.0332503	0.0122095
17	2	2	3	3	0.0331843	0.0120643
18	1.6	1.6	11	11	0.0327966	0.0112346

Table 1.
The electron and ion Kappa-indices affect the values of the effective Debye length and DH potential at fixed values of $r = 0.2$, $\eta = 10^{-3}$, and $Z_{do} = 300$.

more time to attain the Maxwellian equilibrium due to their larger mass compared to electrons.

The effect of dust concentration [denoted through the parameter $\eta(=n_{d0}/n_0)$] is shown on the contours of normalized effective shielding length [as given by Eq. (10)] in **Figure 2** for (a) $\eta = 0$ and (b) $\eta = 10^{-3}$ as function of electron-to-ion temperature ratio in the range $1 \leq T_e/T_i \leq 6$ and electron spectral index $1.6 \leq \kappa_e \leq 5$ at near-Maxwellian ions $\kappa_i = 100$. Since the speed of the test charge is much lower than the dust thermal speed (viz., $v_T \ll v_{Td}$), the test charge is therefore screened by all the plasma species, viz., the electrons, ions, and dust grains, hence effectively modifying the shielding length. The effective shielding length is shown to be decreased in the dusty plasma in comparison with traditional electron-ion plasma and is strongly influenced by the suprathermal tails of electrons. The impact of the superthermal electrons at lower Kappa values is more effective in the case of electron-ion plasma than dusty plasma. In the plots, one can easily observe that light-colored regions correspond to higher values of the effective shielding length while dense-colored regions determine the lower values of the shielding length. However, in **Figure 2(c)** and **(d)**, a reduction in the effective shielding length is revealed by the influence of suprathermal ions at near-Maxwellian electrons

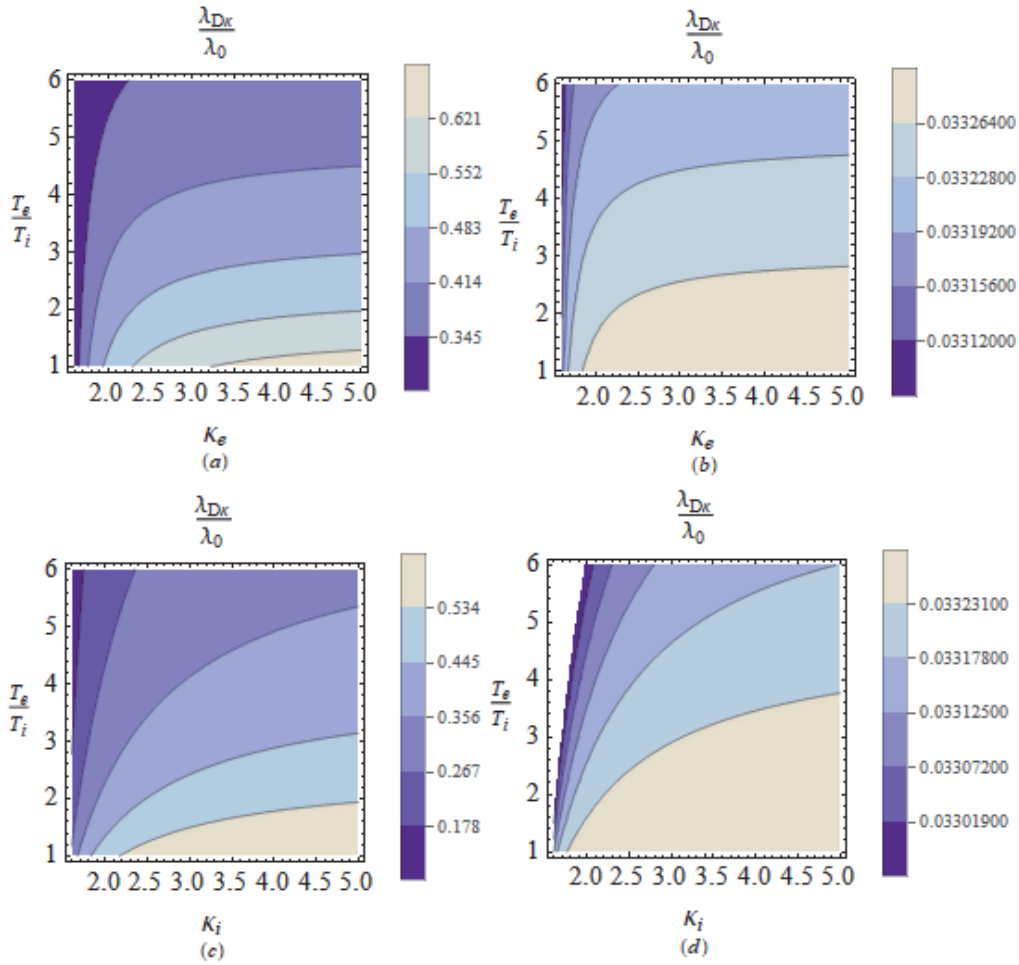

Figure 2.
Contours represent the effective shielding length $\left[\tilde{\lambda}_{D\kappa} = \lambda_{D\kappa}/\lambda_o\right]$ *against the temperature ratio* (T_e/T_i) *and electron spectral index* (κ_e) *for (a)* $\eta(=n_{do}/n_o) \equiv 0$ *(electron-ion plasma) and (b)* $\eta = 10^{-3}$ *(dusty plasma) with* $\kappa_i = 100$ *and* $Z_{do} = 300$. *contours in (c) and (d) vary for* $\tilde{\lambda}_{D\kappa}$ *against the temperature ratio* (T_e/T_i) *and ion spectral index* (κ_i) *for (c)* $\eta = 0$ *(electron-ion plasma) and (d)* $\eta = 10^{-3}$ *(dusty plasma) with* $\kappa_e = 100$ *and* $Z_{do} = 300$. *Other parameters are mentioned in Section 1.4.1.*

$\kappa_e = 100$. It may be noted that due to the variation of electron-to-ion temperature ratio against the ion spectral index, the magnitudes of effective shielding length become smaller at lower values of κ_i than the case of κ_e. However, the effective shielding length approaches to the maximum value in the limit $T_e \simeq T_i$ and decreases by enhancing the electron-to-ion temperature ratios.

4.2 Short-range DH and long-range FF potentials

To study short and long-range shielded potentials of a slowly moving test charge along the z-axis in a Lorentzian dusty plasma, we use Eq. (9) into Eq. (7) and spherical polar coordinates, as $\mathbf{v}_T = (0, 0, v_T)$, $\mathbf{k} = (k\sin\theta_k\cos\varphi_k,\ k\sin\theta_k\sin\varphi_k,\ k\cos\theta_k)$, and $\mathbf{r} = (r\sin\theta_r\cos\varphi_r,\ r\sin\theta_r\sin\varphi_r,\ r\cos\theta_r)$ to finally obtain the total potential $[\phi_1(\mathbf{r},t) = \phi_{DH} + \phi_{FF}]$ as

$$\phi_1(\mathbf{r},t) = \frac{q_T}{r}\exp\left(-\frac{r}{\lambda_{D\kappa}}\right) + \frac{2\sqrt{2}q_T}{\sqrt{\pi}r}\frac{v_T}{v_{Td}}\frac{\xi\lambda_{D\kappa}}{\lambda_{Dd}^2}\frac{\lambda_{D\kappa}^3}{r^3} \tag{11}$$

The first part of Eq. (11) corresponds to the short-range Debye-Hückel (DH) potential, which accounts for the short distances between the test charge and observer, whereas the second part represents the long-range far-field potential in the limit $r \gg \lambda_{D\kappa}$ decaying as the inverse cube of the distance to the test charge. Here $r = \left(\rho^2 + \xi^2\right)^{1/2}$ is the distance from the test charge to observer with radial and axial positions ρ and $\xi(= z - v_T t)$, respectively. When $\kappa_{e,i} \to \infty$, the effective Debye length $\lambda_{D\kappa}$ approaches to λ_D with $c_{\kappa e,i} = 1$, and consequently Eq. (11) exactly coincides with the earlier result [36] in the limit $\cos(\gamma) = \xi/r$, having null dust-charge fluctuations. In **Figure 3**, the magnitude of the effective shielding length varies against the specific ranges of the electron concentration (μ_e) and dust concentration (η) for changing the (a) electron-to-ion temperature ratios $\frac{T_e}{T_i}(= 1, 2, 4, 8)$ at near-Maxwellian electrons and ions $\kappa_{e,i} = 100$ and (b) electron-to-dust temperature ratios $\frac{T_e}{T_d}(= 10, 15, 20, 25)$ with fixed $\frac{T_e}{T_i} = 2$ for Kappa-distributed electrons and ions (i.e., $\kappa_{e,i} = 1.6$), respectively. Note that for an electron-ion plasma, the effective shielding length is approached to unity [35] as the maximum value for isothermal case $\frac{T_e}{T_i} = 1$ (black dotted curve) (see **Figure 3(a)**), which then decreases with respect to the electron concentration. For non-isothermal values, that is, $\frac{T_e}{T_i} = 2$

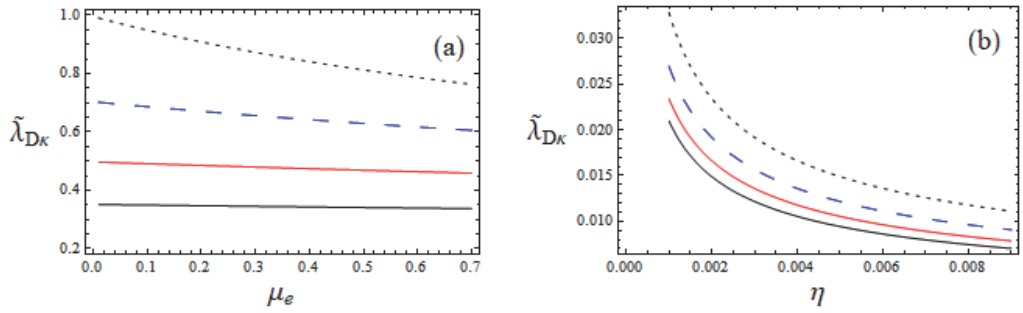

Figure 3.
The shielding length $\tilde{\lambda}_{D\kappa}(= \lambda_{D\kappa}/\lambda_\circ)$ against the electron and dust concentrations (μ_e, η) for varying the temperature ratios $\left(\frac{T_e}{T_i}, \frac{T_e}{T_d}\right)$ in (a) an electron-ion Maxwellian plasma and (b) superthermal dusty plasma, respectively.

(blue dashed curve), 4 (red solid curve), and 8 (black solid curve), the strength of the effective shielding however reduces in terms of fraction showing no more dominant impact of the electron concentration. In the presence of dust component, the effective shielding length is reduced as compared to the electron-ion plasma and clearly depends on the electron-to-dust temperature ratios $\frac{T_e}{T_d}(= 10, 15, 20, 25)$ at $Z_{d0} = 300,$ as can be seen in **Figure 3(b)**.

The variation of the normalized DH potential $\tilde{\phi}_{DH}$ caused by a slowly moving test charge is displayed against the normalized axial distance $\tilde{\xi}$ for varying the dust concentration $\eta = 10^{-3},\ 1.2 \times 10^{-3},$ and 1.4×10^{-3} in **Figure 4** for (a) non-Maxwellian electrons and ions, as well as (b) near-Maxwellian electrons and ions. The DH potentials fastly reduce with a variation of dust concentration and attain large magnitudes in the near-Maxwellian case at $\kappa_{e,i} = 100$ compared to non-Maxwellian case at $\kappa_{e,i} = 1.6$.

Figure 5 exhibits how suprathermal electrons and ions modify the profiles of long-range FF potential $(\tilde{\phi}_{FF})$ caused by a slow test charge moving with speed $v_T = 0.02 v_{Td}$. For small values of electron spectral index $\kappa_e (= 1.6, 1.8)$, the shielded FF potentials are more localized than the case at near-Maxwellian electrons for $\kappa_e = 100$ (see the red solid curve in **Figure 5(a)**). However, the magnitudes of the FF potential are comparatively decreased in **Figure 5(b)** because of the strong contribution of suprathermal ions.

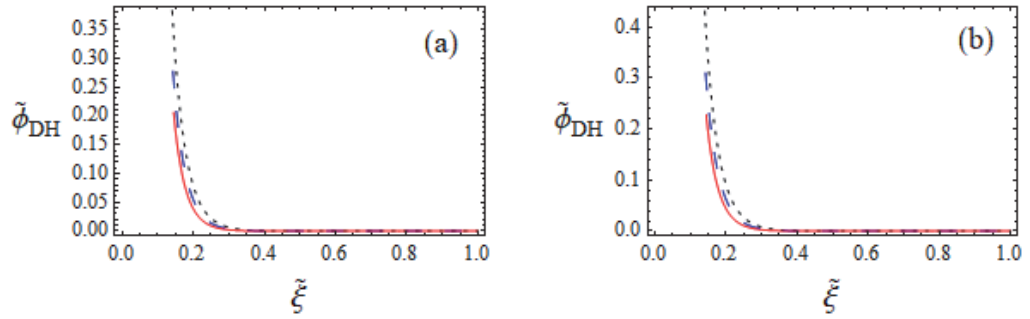

Figure 4.
The DH potential $\tilde{\phi}_{DH}\left[= \phi_{DH}/(q_T/\lambda_o)\right]$ vs. the axial distance $\tilde{\xi}(= \xi/\lambda_o)$ for different dust concentrations $\eta = 10^{-3}$ (black dotted curve), 1.2×10^{-3} (blue dashed curve), and 1.4×10^{-3} (red solid curve) at $Z_{do} = 200$ and $\tilde{\rho} = 0$ with (a) $\kappa_{e,i} = 1.6$ and (b) $\kappa_{e,i} = 100$.

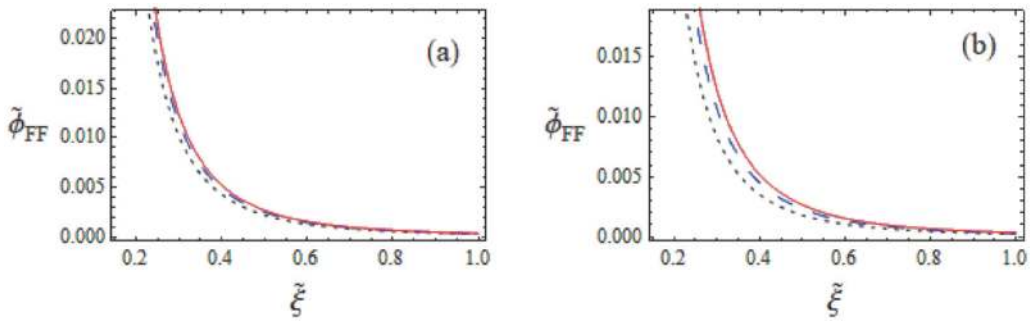

Figure 5.
The FF potential $\tilde{\phi}_{FF}\left[= \phi_{FF}/(q_T/\lambda_o)\right]$ vs. $\tilde{\xi}$ for varying (a) $\kappa_e = 1.6$ (black dotted curve), 1.8 (blue dashed curve), and 100 (red solid curve) with $\kappa_i = 100$, and (b) $\kappa_i = 1.6$ (black dotted curve), 1.8 (blue dashed curve), and 100 (red solid curve) with $\kappa_e = 100$. other values are $\eta = 10^{-4}$, $\rho = 0$, and $Z_{do} = 300$.

4.3 Resonating test charge response

To examine the resonant interaction of a test charge with DA waves, we first simply derive the dielectric constant of the DA waves using the limit $v_{Td} \ll \omega/k \ll \theta_{Te}, \theta_{Ti}$ in Eq. (8). We therefore consider the small and large argument expansions $C_s \ll 1$ and $C_d \gg 1$ of the plasma dispersion functions. On DA scales, the inertia is mainly provided by the negatively charged dust grains and restoring force by the pressures of superthermal inertialess electrons and ions for maintaining the propagation of DA waves. In typical laboratory plasmas, the frequency of DA waves is often below the dust plasma oscillation frequency in the range of 1–100 Hz. Thus, the modified dielectric constant for a Lorentzian dusty plasma takes the following form

$$D(k, \mathbf{k}\cdot\mathbf{v}_T) = 1 + \frac{1}{k^2\lambda_D'^2} - \frac{\omega_{pd}^2}{(\mathbf{k}\cdot\mathbf{v}_T)^2}. \tag{12}$$

The effective Debye length now gets a new form $\lambda_D' = \lambda_0/\sqrt{B_\kappa}$ with $B_\kappa = c_{\kappa e}\frac{n_{e0}}{n_0} + c_{\kappa i}\frac{T_e}{T_i}$. Note that dust-charge fluctuations are also ignored here because the characteristic damping rate attributed to dust charge fluctuations is much smaller than the collisional and Landau damping rates. The reciprocal of Eq. (12) can be simplified as

$$D^{-1} = \frac{k^2\lambda_0^2}{B_\kappa + k^2\lambda_0^2}\left\{1 + \frac{\omega_D^2}{(\mathbf{k}\cdot\mathbf{v}_T)^2 - \omega_D^2}\right\}, \tag{13}$$

with

$$\omega_D = \frac{kC_D}{\left(B_\kappa + k^2\lambda_0^2\right)^{1/2}}. \tag{14}$$

This is the DA resonance frequency with DA speed $C_D\left(=\omega_{pd}\lambda_0\right)$. For long wavelength limit $k\lambda_0 \ll B_\kappa$, the DA frequency reduces to $\omega_D = kC_D/\sqrt{B_\kappa}$ in the Lorentzian dusty plasma, while in the short wavelength limit $k\lambda_0 \gg B_\kappa$, the frequency simply approaches to the dust plasma oscillation frequency $\omega_D \simeq \omega_{pd}$. The factor $\omega_D^2/\left\{(\mathbf{k}\cdot\mathbf{v}_T)^2 - \omega_D^2\right\}$ in Eq. (13) identifies the dynamical effects of dust grains, which may lead to an oscillatory WF potential strongly depending upon whether the product $\mathbf{k}\cdot\mathbf{v}_T$ is smaller or larger than ω_D.

4.4 Short-range DH and long-range WF potentials

For static or slowly moving test charge in a Lorentzian dusty plasma, its potential distributions are found spherically symmetric both in the axial and radial directions. Consequently, the DH and FF shielded potentials are appropriately solved with spherical polar coordinates. However, if the test charge moves with finite speed in a specific direction along the z-axis, the resonant interaction of test charge with the DA wave leads to the asymmetric distribution of potential in the form of WF behind the test charge. The plasma model is then preferably solved in cylindrical coordinates. Thus, following the standard techniques [37, 38, 40] for DH and WF potentials, we make use of Eq. (13) into Eq. (7) to finally arrive at

$$\phi_1(\mathbf{r},t) = \frac{q_T}{r}\exp\left(-\frac{r\sqrt{B_\kappa}}{\lambda_0}\right) + \frac{2q_T}{\xi}\left(1+\frac{C_D^2}{B_\kappa v_T^2}\right)\left(B_\kappa - \frac{C_D^2}{v_T^2}\right)^{-1}\cos\left(\frac{\omega_{pd}\xi}{\sqrt{B_\kappa}v_T}\right), \tag{15}$$

where $\xi(=r_\parallel - v_T t)$ is the axial distance between the test charge and observer. The first part on the right hand side of Eq. (15) shows the contribution of modified DH potential and the second part corresponds to oscillatory WF potential accounting for the suprathermal electrons and ions in a Lorentzian dusty plasma. For $v_T > C_D$ and $\cos\left(\omega_{pd}\xi/v_T\sqrt{B_\kappa}\right) < 0$, the WF potential becomes attractive [40] and dominates over the repulsive DH potential because the latter decreases rapidly beyond the shielding cloud. An oscillatory WF potential $\tilde{\phi}_{WF}(=\phi_{WF}\lambda_0/q_T)$ of a test charge moving with speed $v_T = 0.2C_D$ is shown along the axial direction $\tilde{\xi}$ as a function of spectral indices κ_e and κ_i in **Figure 6(a)** and **(b)**, respectively. Observe that the amplitude of the WF potential increases as the superthermal indices κ_e and κ_i increase at fixed $\eta = 10^{-3}$ and $Z_{d0} = 300$. Moreover, the wakefield damps behind the test charge a bit earlier as shown in **Figure 6(b)** due to the strong dependence of suprathermal ions on the effective shielding length in comparison with the suprathermal electrons. The impact of electron-to-ion temperature ratio is also examined on the profiles of WF and DH potentials as a function of axial distance $\tilde{\xi}$

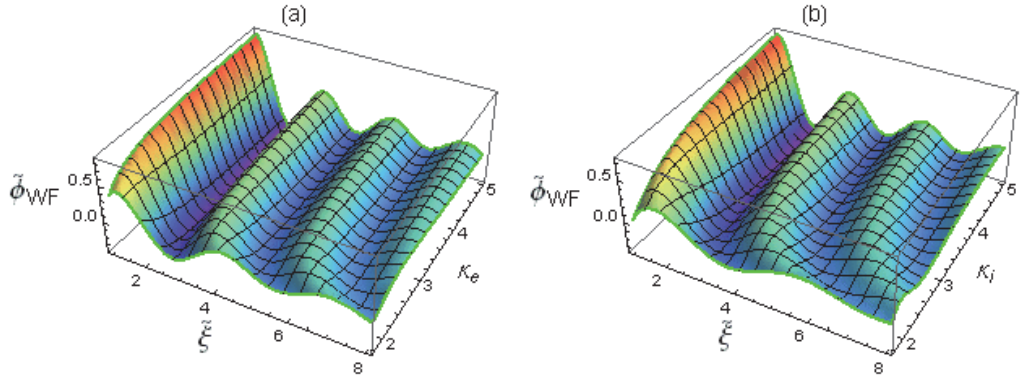

Figure 6.
The normalized WF potential $\tilde{\phi}_{WF}$ as a function of $\tilde{\xi}$ for varying the spectral indices as (a) $1.8 \le \kappa_e < 5$ with fixed $v_T = 0.2C_D$ and $\kappa_i = 100$, and (b) $1.8 \le \kappa_i < 5$ with $v_T = 0.2C_D$ and $\kappa_e = 100$.

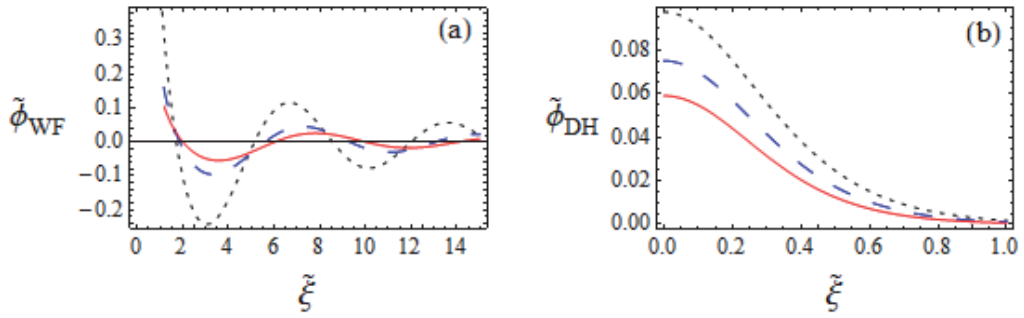

Figure 7.
The WF and DH potentials are shown against the axial distance $\tilde{\xi}$ for changing temperature ratios (a) T_e/T_i =2 (black dotted curve), 2.5 (blue dashed curve), and 3 (red solid curve), and (b) T_e/T_i =2 (black dotted curve), 2.5 (blue dashed curve), and 3 (red solid curve), respectively. Other common parameters are $\kappa_{e,i} = 1.6$, $v_T = 0.2C_D$, $\eta = 10^{-3}$, and $Z_{do} = 100$.

with fixed radial distance $\rho = 0.54\lambda_0$ and $v_T = 0.2C_D$ as can be seen in **Figure 7(a)** and **(b)**, respectively. It is important to examine that electron-to-ion temperature ratio suppresses the magnitudes of the WF and DH potentials at low values of $\kappa_{e,i} = 1.6$ in the Lorentzian dusty plasma (**Figures 6** and 7).

4.5 Fast moving test charge response

In this case, the test charge is assumed to be moving much faster than all the plasma species (viz., the electrons, ions and negatively charged dust grains). Consequently, Eq. (6) can be expressed in 1D form to finally arrive at $D(k, \mathbf{k}.\mathbf{v}_T) \simeq 1$ in the limits $v_T| \gg ku_j$ and $\omega = \mathbf{k}.\mathbf{v}_T$. Thus, the test charge potential (7) simply leads to the Coulomb potential

$$\phi_1(\mathbf{r}, t) = \phi_C \equiv \frac{q_T}{r}. \tag{16}$$

It is now clear that if the test charge is moving very fast, then there is no shielding around it in the Lorentzian dusty plasma.

5. Conclusion

To conclude, we have briefly discussed different plasma diagnostic techniques and specifically investigated the novel features of interaction potentials caused by a test charge moving with constant velocity $\mathbf{v}_T$ along the z-axis in a collisionless unmagnetized Lorentzian dusty plasma. For this purpose, the linearized coupled Vlasov-Poisson equations are employed to model suprathermal electrons and ions with Kappa-df, as well as negatively charged dust grains with Maxwell-df, respectively. After applying the space-time Fourier transformations, an electrostatic potential is obtained with a modified dielectric constant. For taking the test charge speed much smaller than the dust thermal speed in a Lorentzian dusty plasma, we then express the total potential distribution in terms of short-range Debye-Hückel (DH) and long-range far-field potentials. The DH potential exponentially decays with distance, whereas FF potential decreases as the inverse cube of the distance. Both the potentials are substantially influenced by the plasma and superthermality parameters. However, a resonating test charge with DA oscillations introduces the long-range WF potential excitations behind the test charge in Lorentzian dusty plasmas. A Coulomb potential is obtained when the test charge is moving very fast compared to plasma species, and there is no shielding around it in the Lorentzian dusty plasma.

Vladimirov and Nambu [40] have already utilized the idea of WF potential for making new materials by attracting the same polarity dust grains in dusty plasmas. The physics of attractive forces between the negatively charged dust grains is completely analogous to that of Cooper pairing of electrons in superconductors [59]. The dust particle physically polarizes the plasma medium and creates attractive potential regions, where positive ions from collective interaction of DA waves can be focused. This may in turn lead to the possibility for dust crystallization and dust coagulation in both laboratory and space dusty plasmas.

Acknowledgements

Dr. S. Ali dedicates this document to Late Prof. P.K. Shukla and Dr. B. Eliasson (University of Strathclyde, UK) who were very kind to him at many occasions

during discussions on dusty plasmas, and acknowledges the partial financial assistance from USTC, Hefei, China, and ICTP, Trieste, Italy, for making his visits feasible in 2018 and 2019, respectively. Professor Y. Al-Hadeethi also acknowledges the technical support of the Deanship of Scientific Research (DSR), King Abdulaziz University, Saudi Arabia.

Author details

Shahid Ali[1*] and Yas Al-Hadeethi[2]

1 National Centre for Physics (NCP), Quaid-e-Azam University Campus, Islamabad, Pakistan

2 Faculty of Sciences, Department of Physics, King AbdulAziz University, Jeddah, Saudia Arabia

*Address all correspondence to: shahid_gc@yahoo.com

References

[1] Al-Hadithi Y, Tallents GJ, Neely D. X-Ray Lasers 1990. Bristol: IOP Publishers; 1991

[2] Al-Hadithi Y, Tallents GJ, Zhang J, Key MH, Norreys PA, Kodama R. Energy transport in plasmas produced by a high brightness Krypton fluoride laser focused to a line. Physics of Plasmas. 1994;**1**:1279. DOI: 10.1063/1.870726

[3] Al-Hadeethi Y, Al-Mujtabi A, Al-Marzouki FM. Laser produced plasma x-ray sources for nanoscale resolution contact microscopy: A candidate in cancerous stem cells imaging. Advances in Molecular Imaging. 2017;**7**:67. DOI: 10.4236/ami.2017.74004

[4] Chen FF. Introduction to Plasma Physics and Controlled Fusion. New York: Plenum; 1984

[5] Fortov VE, Ivlev AV, Khrapak SA, Morfill GE. Complex (dusty) plasmas: Current status, open issues, perspectives. Physics Reports. 2005;**421**:1. DOI: 10.1016/j.physrep.2005.08.007

[6] Shukla PK, Silin VP. Dust ion-acoustic wave. Physica Scripta. 1992;**45**:508. DOI: 10.1088/0031-8949/45/5/015

[7] Rao NN, Shukla PK, Yu MY. Dust-acoustic waves in dusty plasmas. Planetary Space Science. 1990;**38**:543. DOI: 10.1016/0032-0633(90)90147-I

[8] Barkan A, D'Angelo N, Merlino RL. Experiments on ion-acoustic waves in dusty plasmas. Planetary Space Science. 1996;**44**:239. DOI: 10.1016/0032-0633(95)00109-3

[9] Merlino RL, Barkan A, Thompson C, D'Angelo N. Laboratory studies of waves and instabilities in dusty plasmas. Physics of Plasmas. 1998;**5**:1607. DOI: 10.1063/1.872828

[10] Barkan A, Merlino RL, D'Angelo N. Laboratory observation of the dust-acoustic wave mode. Physics of Plasmas. 1995;**2**:3563. DOI: 10.1063/1.871121

[11] Krall NA, Trivelpiece AW. Principles of Plasma Physics. New York: McGraw-Hill; 1973

[12] Neufeld J, Ritchie RH. Passage of charged particles through plasma. Physical Review. 1955;**98**:1632. DOI: 10.1103/PhysRev.98.1632

[13] Montgomery D, Joyce G, Sugihara R. Inverse third power law for the shielding of test particles. Plasma Physics. 1968;**10**:681. DOI: 10.1088/0032-1028/10/7/304

[14] Stenflo L, Yu MY, Shukla PK. Shielding of a slow test charge in a collisional plasma. Physics of Fluids. 1973;**16**:450. DOI: 10.1063/1.1694361

[15] Shukla PK, Spatschek K-H. Shielding of a moving test charge in a turbulent plasma. Physics Letters A. 1973;**44**:398. DOI: 10.1016/0375-9601(73)90840-2

[16] Yu MY, Stenflo L, Shukla PK. On the electric field of a moving test charge. Radio Science. 1972;**7**:1151. DOI: 10.1029/RS007i012p01151

[17] Shukla PK, Spatschek K-H, Yu MY. Far-field potential of a test charge in an inhomogeneous and magnetized plasma. Canadian Journal of Physics. 1974;**52**:281. DOI: 10.1139/p74-040

[18] Ali S, Nasim MH, Murtaza G. Effects of dust-charge fluctuations on the potential of an array of projectiles in a partially ionized dusty plasma. Physics of Plasmas. 2003;**10**:4207. DOI: 10.1063/1.1619976

[19] Ali S, Nasim MH, Murtaza G. Correlation effects due to an axial

propagation of projectiles in a dusty plasma. Physics of Plasmas. 2005;**12**: 033502. DOI: 10.1063/1.1844496

[20] Ali S, Murtaza G, Nasim MH. Energy loss for the assemblies of charged projectiles in a dusty plasma. Physics of Plasmas. 2005;**12**:072104. DOI: 10.1063/1.1933739

[21] Brandt W, Ratkowski A, Ritchie RH. Energy loss of swift proton clusters in solids. Physical Review Letters. 1974;**33**: 1325. DOI: 10.1103/PhysRevLett.33.1325

[22] Deutsch C, Tahir NA. Fragmentation and stopping of heavy cluster ions in a lithium target—Application to target implosion. Physics of Fluids B. 1992;**4**:3735. DOI: 10.1063/1.860329

[23] Skupsky S. Energy loss of ions moving through high-density matter. Physical Review A. 1977;**16**:727. DOI: 10.1103/PhysRevA.16.727

[24] Li CK, Petrasso RD. Charged-particle stopping powers in inertial confinement fusion plasmas. Physical Review Letters. 1993;**70**:3059

[25] Lindl JD. Inertial Confinement Fusion. New York: Springer Verlag; 1998

[26] Jones ME, Keinigs R. Ion plasma wave wakefield accelerators. IEEE Transactions on Plasma Science. 1987; **15**:203. DOI: 10.1109/TPS.1987.4316686

[27] Mohideen U, Rahman HU, Smith MA, Rosenberg M, Memdis DA. Intergrain coupling in dusty-plasma Coulomb crystals. Physical Review Letters. 1998;**81**:349. DOI: 10.1103/PhysRevLett.81.349

[28] Takahashi K, Oishi T, Shimomai K-I, Hayashi Y, Nishino S. Analyses of attractive forces between particles in Coulomb crystal of dusty plasmas by optical manipulations. Physical Review E. 1998;**58**:7805. DOI: 10.1103/PhysRevE.58.7805

[29] Zwicknagel G, Deutsch C. Correlated ion stopping in plasmas. Physical Review E. 1997;**56**:970. DOI: 10.1103/PhysRevE.56.970

[30] Sanmartin JR, Lam SH. Far-wake structure in rarefield plasma flows past charged bodies. Physics of Fluids. 1971; **14**:62. DOI: 10.1063/1.1693289

[31] Yu MY, Tegeback R, Stenflo L. On test charge potentials in collisional plasmas. Zeitschrift für Physik. 1973; **264**:341. DOI: 10.1007/BF01398860

[32] Peter T. Linearized potential of an ion moving through plasma. Journal of Plasma Physics. 1990;**44**:269. DOI: 10.1017/S0022377800015178

[33] Shivamoggi BK, Mulser P. Dielectric screening and stopping power of a test charge moving in a plasma. Journal of Plasma Physics. 1998;**60**:819

[34] Shukla PK, Singh RN. Total energy loss of a test charge in a collisional magnetoplasma. Physica Scripta. 1971;**4**: 282. DOI: 10.1088/0031-8949/4/6/008

[35] Lakshmi VS, Bharuthram R, Shukla PK. Debye shielding in a dusty plasma. Astrophysics and Space Science. 1993;**209**:213. DOI: 10.1007/BF00627441

[36] Shukla PK. Shielding of a slowly moving test charge in dusty plasmas. Physics of Plasmas. 1994;**1**:1362. DOI: 10.1063/1.870736

[37] Nambu M, Akama H. Attractive potential between resonant electrons. Physics of Fluids. 2300;**1985**:28. DOI: 10.1063/1.865284

[38] Nambu M, Vladimirov SV, Shukla PK. Attractive forces between charged particulates in plasmas. Physics

Letters A. 1995;**203**:40. DOI: 10.1016/0375-9601(95)00380-L

[39] Shukla PK, Rao NN. Coulomb crystallization in colloidal plasmas with streaming ions and dust grains. Physics of Plasmas. 1996;**3**:1770. DOI: 10.1063/1.871695

[40] Vladimirov SV, Nambu M. Attraction of charged particles in plasmas with finite flows. Physical Review E. 1995;**52**:R2172. DOI: 10.1103/PhysRevE.52.R2172

[41] Nambu M, Saikia BJ, Hada T. Wake potential around a test dust particulate in a magnetized plasma with streaming ions. Journal of the Physical Society of Japan. 2001;**70**:1175. DOI: 10.1143/jpsj.70.1175

[42] Freund HP, Smith RA, Papadopoulos K, Palmadesso P. Modulational instability in a plasma with supra-thermal electrons. Physics of Fluids. 1981;**24**:442. DOI: 10.1063/1.863390

[43] Freese KB, Walsh JE, Lohr J. Wave-particle interaction in the late beam-plasma instability. Physics of Fluids. 1979;**22**:2367. DOI: 10.1063/1.862549

[44] Smith RA, Goldstein ML, Papadopoulos K. Nonlinear stability of solar type III radio bursts. I-Theory. The Astrophysical Journal. 1979;**234**:348

[45] Van Compernolle B, Gekelman W, Pribyl P. Generation of supra-thermal electrons and Alfvén waves by a high power pulse at the electron plasma frequency. Physics of Plasmas. 2006;**13**:092112. DOI: 10.1063/1.2261850

[46] Eliasson B, Shao X, Milikh G, Mishin EV, Papadopoulos K. Numerical modeling of artificial ionospheric layers driven by high-power HF heating. Journal of Geophysical Research. 2012;**117**:A10321. DOI: 10.1029/2012JA018105

[47] Vasyliunas VM. A survey of low-energy electrons in the evening sector of the magnetosphere with OGO 1 and OGO 3. Journal of Geophysical Research. 1968;**73**:2839. DOI: 10.1029/JA073i009p02839

[48] Summers D, Thorne RM. The modified plasma dispersion function. Physics of Fluids B. 1991;**3**:1835. DOI: 10.1063/1.859653

[49] Baluku TK, Hellberg MA. Dust acoustic solitons in plasmas with kappa-distributed electrons and/or ions. Physics of Plasmas. 2008;**15**:123705. DOI: 10.1063/1.3042215

[50] Ali S, Eliasson B. Slowly moving test charge in two-electron component non-Maxwellian plasma. Physics of Plasmas. 2015;**22**:084508. DOI: 10.1063/1.4928901

[51] Ali S, Eliasson B. Slow test charge response in a dusty plasma with kappa distributed electrons and ions. Physica Scripta. 2017;**92**:084003. DOI: 10.1088/1402-4896/aa7c09

[52] Burton FD, Conte SD. The Plasma Dispersion Function. New York: Academic Press; 2015

[53] Debye P, Hückel E. On the Debye length in strong electrolytes. Physikalische Zeitschrift. 1923;**24**:185

[54] Rubab N, Murtaza G. Debye length in non-Maxwellian plasmas. Physica Scripta. 2006;**74**:145. DOI: 10.1088/0031-8949/74/2/001

[55] Du J, Guo R, Liu Z, Du S. Slowing down of charged particles in dusty plasmas with power-law kappa-distributions. Contributions to Plasma Physics. 2019;**59**:144. DOI: 10.1002/ctpp.201800046

[56] Wahlund J-E, Andre M, Eriksson AIE, Lundberg M, Morooka MW, Shafiq M, et al. Detection of dusty plasma near the

E-ring of Saturn. Planetary and Space Science. 2009;**57**:1795. DOI: 10.1016/j.pss.2009.03.011

[57] Leisner JS, Russell CT, Dougherty MK, Blanco-Cano X, Strangeway RJ, Bertucci C. Ion cyclotron waves in Saturn's E ring: Initial Cassini observations. Geophysical Research Letter. 2006;**33**:L11101. DOI: 10.1029/2005GL024875

[58] Kurth WS, Averkamp TF, Gurnett DA, Wang Z. Cassini RPWS observations of dust in Saturn's E Ring. Planetary and Space Science. 2006;**54**: 988. DOI: 10.1016/j.pss.2006.05.011

[59] De Gennes PG. Superconductivity of Metals and Alloys. New York: Benjamin; 1966